Observation of a magneto-Rayleigh-Taylor instability in magnetically collimated plasma jets

S. Malko [1,*] D. B. Schaeffer [2] W. Yao [3,4] V. Valenzuela-Villaseca [5] C. Johnson [1,5] G. Fiksel [6] A. Ciardi [4] and W. Fox [1,5]

[1] *Princeton Plasma Physics Laboratory, 100 Stellarator Road, Princeton, New Jersey 08540, USA*

[2] *Department of Physics & Astronomy, University of California–Los Angeles, Los Angeles, California 90095, USA*

[3] *LULI-CNRS, CEA, Sorbonne Université, Ecole Polytechnique, Institut Polytechnique de Paris, F-91128 Palaiseau Cedex, France*

[4] *Sorbonne Université, Observatoire de Paris, Université PSL, CNRS, LERMA, F-75005 Paris, France*

[5] *Department of Astrophysical Sciences, Princeton University, Princeton, New Jersey 08544, USA*

[6] *Center for Ultrafast Optical Science, University of Michigan, Ann Arbor, Michigan 48109, USA*

(Received 16 November 2023; accepted 5 June 2024; published 27 June 2024)

We present the direct experimental observation of the formation of a diamagnetic cavity and magneto-Rayleigh-Taylor (MRT) instability in a $\beta \approx 1$ high energy density plasma. Proton radiography is used to measure the two dimensional path-integrated magnetic field in a laser-produced plasma propagating parallel to a preimposed magnetic field. Flutelike structures, associated with the MRT instability, are observed to grow at the surface of the cavity, with a measured wavelength of 1.2 mm and growth time of 4 ns. These measurements are in good agreement with predictions of three dimensional magnetohydrodynamic simulations using the GORGON code.

DOI: 10.1103/PhysRevResearch.6.023330

I. INTRODUCTION

The transport properties of magnetic fields in plasmas have been extensively studied over the last two decades. The active magnetospheric particle tracer experiment (AMPTE) [1] studied artificial comets by releasing barium ions to expand across the ambient magnetic field of the Earth's magnetosphere. These experiments observed the creation of diamagnetic cavities and flutelike structures associated with magneto-Rayleigh-Taylor (MRT) instabilities [2–4]. Such processes are present in astrophysical phenomena in scaled experiments such as magnetic reconnection [5–8] and generation of magnetized collisionless shocks [9–12]. Additionally, the magnetic field exerts forces back on the expanding plasma, which can collimate plasma flows [13,14], and so has been proposed to collimate astrophysical jets [15,16].

When an expanding plasma pushes against a background magnetic field, it displaces the field out of its volume and forms a diamagnetic cavity. This expansion occurs until the equipartition of vacuum and magnetic pressure at the plasma's outer boundary is reached, which determines the cavity's maximum radius R_b. These systems can be unstable to the MRT instability, leading to the generation of field-aligned flute structures at the cavity edge. An important dynamical parameter that influences the type of instability supported in the cavity is the ratio of the directed ion gyroradius of expanding ions, ρ_i, to R_b [17]. Here, $\rho_i = v_d/\omega_{ci}$, where $\omega_{ci} = ZeB/m_i$ is the ion gyrofrequency, v_d is the expansion velocity, and Z and m_i are the ion charge and mass.

The MRT instability can occur when a magnetic field is used to directly accelerate or compress a plasma, as seen in Z pinches and MagLIF [18–20], or when an expanding plasma is decelerated by a surrounding magnetic field [15,21,22]. Numerical simulations of these processes are notoriously challenging, requiring magnetohydrodynamic (MHD) codes with accurate descriptions of the plasma-vacuum interface. Detailed laboratory measurements of MRT and diamagnetic cavities in various ρ_i/R_b regimes are necessary for benchmarking MHD simulations [15,16].

Most experimental measurements have been conducted in regimes where $\rho_i/R_b \approx 1$ [17,23–25], or even exceeding this value [26], which is of particular interest due to its relevance to space observations [1]. The regime where $\rho_i/R_b < 1$, pertinent to astrophysical objects [15] and high-current Z pinches [18,19], remains largely unexplored. Recent experiments have been conducted in the regime of $\rho_i/R_b \approx 0.1 - 1$ [13,14,27], where extended magnetohydrodynamics (MHD) effects are becoming significant. In this regime Khiar *et al.* [14] observed plasma density structures related to MRT instabilities using optical interferometry. However, direct measurements of magnetic field evolution are particularly crucial in this case, as the magnetic field may evolve independently from the plasma, challenging the assumptions of ideal MHD. Such measurements are essential for benchmarking extended MHD simulation codes used in the design of high-energy density plasma and inertial confinement fusion experiments.

In this Letter, we report direct 2D measurements of the magnetic field dynamics in expanding laser-driven plasma using proton radiography. These new measurements are in a regime of $\rho_i/R_b \approx 0.1$, which has been poorly experimentally investigated until now. The results confirm the magnetic

*Contact author: smalko@pppl.gov

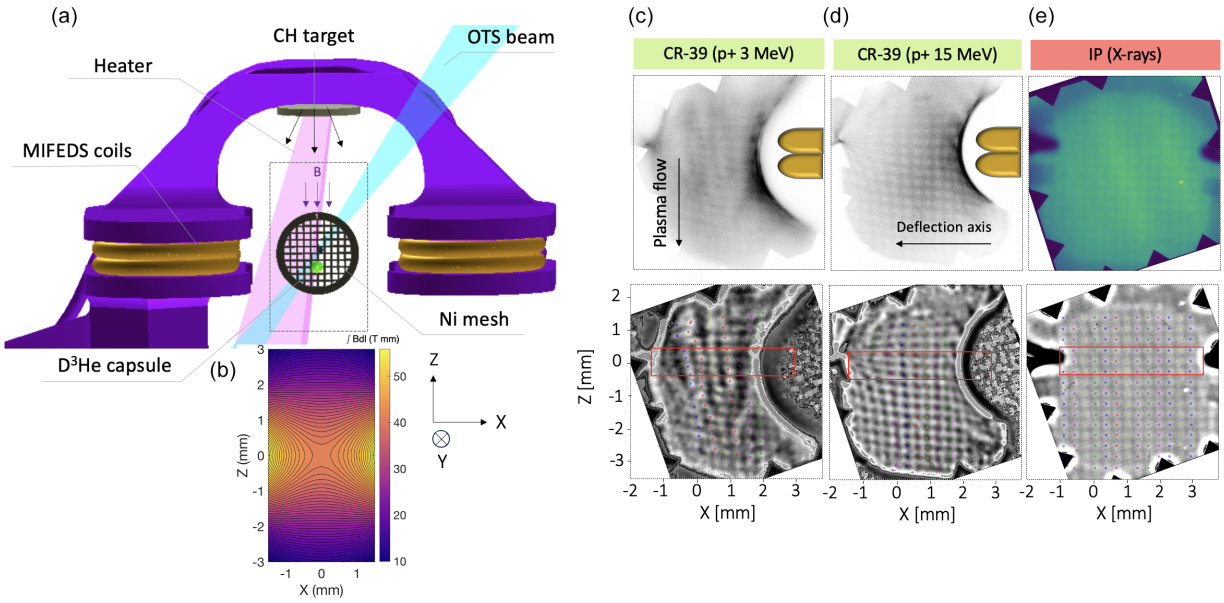

FIG. 1. (a) Experimental setup. The z axis is the direction of the initial magnetic field and the plasma flow. The proton deflectometry beam propagates along the y axis, leading to proton deflections largely along the x axis. (b) Vacuum path-integrated magnetic field calculated by COMSOL. Raw images from proton radiography detector stacks in the xz plane obtained at 20 ns plasma expansion time: CR39 for 3 (c) and 15 MeV (d) protons; (e) Image plate (IP) for x-rays. The bottom panel shows corresponding post-processed scaled images in the plasma plane with identified beamlet positions. The midplane region between MIFEDS coils is indicated as the area outlined in red.

nature of cavity formation and instabilities—previously observed only through density evolution [14]. Furthermore, our results demonstrate magnetic collimation and MRT development in a plasma expanding parallel to the field, a critical aspect of jet collimation [15]. The experimental data is in remarkable agreement with the diamagnetic cavity evolution, jet collimation, and MRT dynamics predicted by MHD simulations [15].

II. EXPERIMENT

The experiments were performed at the University of Rochester Laboratory for Laser Energetics (LLE) OMEGA Laser Facility [28]. A 20 J heater beam with a 1 ns pulse duration was used to ablate a 20 μm thick plastic target (CH), generating a plasma plume propagating predominantly parallel to a preimposed magnetic field. The quasistatic magnetic field was produced by the magnetoinertial fusion electrical discharge system (MIFEDS) [29], which delivered ≈3.25 T at the midpoint between two coils over a volume of 5 mm^3. The magnetic field was modeled using COMSOL and exhibited some spatial nonuniformity due to the coil design. The field strength was at its minimum at the midpoint and increased in the direction of each coil, as shown in Fig. 1(b). A 2ω beam of 30 J energy and 1 ns pulse duration was used for optical Thomson scattering (OTS) for measuring the local plasma electron density and temperature [30].

The magnetic field in the region between the coils was measured as a function of the expansion time using proton radiography [31]. On each experiment, an imploded D^3He-filled capsule produced an isotropic point source (20–50 μm radius) of 3 MeV and 14.7 MeV protons as fusion products, as well as continuum x-rays with 10–30 keV energies [32]. The capsule was positioned at a distance $L_1 = 10$ mm from the target chamber center (TCC), along the proton radiography axis, and a detector stack positioned at a distance $L_2 = 154$ mm on the opposite side of TCC. The proton beam was split into several beamlets using a Ni mesh with a pitch of 125 μm, positioned 4 mm from the capsule. We employed simultaneous proton and x-ray radiography to obtain an accurate *in situ* reference for the position of undeflected beamlets [33,34]. Figures 1(c)–1(e) (top panel) show examples of the raw radiography data obtained with a detector stack. This stack consisted of two CR-39 detectors for protons [32] and an image plate (IP) for x-rays. The images were further post processed, as shown in the bottom panel, to enhance contrast, cross-align using the teeth-border frame, and identify beamlet positions.

The path-integrated magnetic field was calculated using the standard theory of proton deflectometry [35] $\int d\vec{l} \times \vec{B} = \frac{m_p v_p}{e} \frac{L_1+L_2}{L_1 L_2} (\vec{d}_2 - \vec{d}_1)$, where m_p is the proton mass, v_p is the proton speed, e is the electric charge, d_2 is the deflected beamlet position obtained from the proton image, and d_1 is the undeflected beamlet position obtained from the x-ray image. Here, both d_1 and d_2 are given in terms of the coordinate system of the plasma plane, which is related to the observation on the detector by the magnification $M = (L_1 + L_2)/L_1$. A detailed explanation of this diagnostic technique is presented in [33,34]. There is no significant contribution of an electric field to the deflection of the protons since the electric field strength is negligible for these experiments. This assumption was also confirmed in the magnetic field data analysis.

In Fig. 2, we present (a) the initial two-dimensional path-integrated magnetic field $\int B dl_{\text{vac}}$ in the region of interest, calculated using a COMSOL model validated against shots with a vacuum magnetic field and no plume [33], and (b) the experimental measurement $\int B dl$ at 30 ns expansion

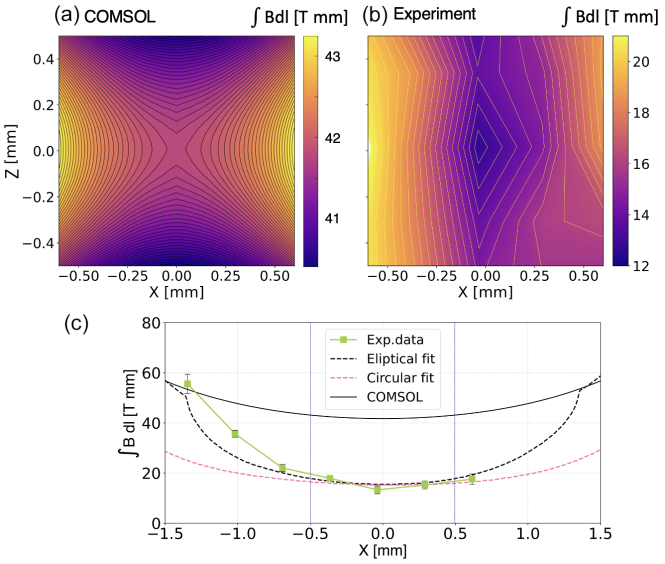

FIG. 2. (a) 2D vacuum path-integrated magnetic field calculated by COMSOL $\int Bdl_{\text{vac}}$ in the region of interest. (b) 2D map of measured path-integrated magnetic field $\int Bdl$ by 15 MeV proton radiography at 30 ns. (c) 1D path-integrated magnetic field as a function of x extracted from (a) and (b) in the midplane region $z = -0.3$ to 0.3 mm. The $\int Bdl$ is averaged over three midplane beamlet rows. The error bar consists of standard deviation of the signal for each data point and systematic error of 0.9 T.

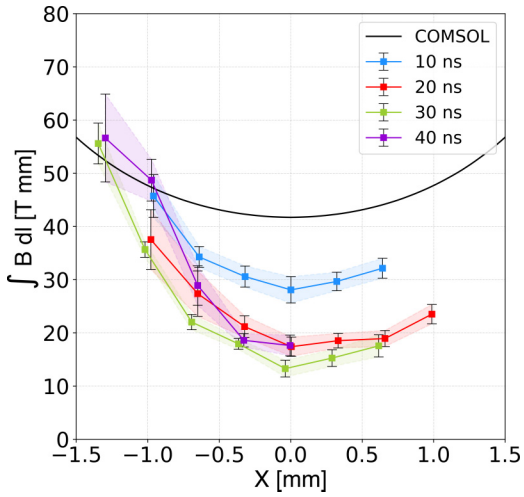

FIG. 3. 1D path-integrated magnetic field $\int Bdl$ as a function of position x along the deflection axis in the midplane region $z = -0.3$ to 0.3 mm extracted from 2D $\int Bdl$ maps produced by 15 MeV protons at each plasma expansion time. The $\int Bdl$ is averaged over three midplane beamlet rows.

time. The values of $\int Bdl$ were calculated from the beamlet deflections. Comparing (a) and (b), we observe a significant overall decrease in magnetic field within the volume, indicating diamagnetic field expulsion. Figure 2(c) shows the comparison of horizontal 1D lineouts of measured $\int Bdl$ and $\int Bdl_{\text{vac}}$ in the midplane, where we can observe a reduction in $\int Bdl$ of nearly 50%. We find that the experimental $\int Bdl$ can be fit by an elliptical cavity model, where we introduce a zero magnetic field ($B = 0$ T) within an ellipse of compressed field defined by minor axis a and major axis b in COMSOL 2D map in xy plane. The best agreement with the observed $\int Bdl$ is obtained using a model with $a = 1.6 \pm 0.3$ mm and $b = 2.5 \pm 0.3$ mm [Fig. 2(c)]. The ellipticity of the cavity is necessary because the apparent width in the x direction, representing the radius from $x = 0$ to where $\int Bdl$ matches $\int Bdl_{\text{vac}}$ at $x = 1$–1.5 mm, differs from the required "excavation length" in the direction of line integration needed to match the minimum value of $\int Bdl$ at $x = 0$. This is demonstrated with a circular model with $r = 2.5$ mm, which matches the value at $x = 0$ but does not account for the excavation length. The 2D path-integrated magnetic field map does not show any evidence of self-generated Biermann battery fields. We do not expect these fields to be dominant, as our measurements were performed 5 mm away from the laser-target interaction point and tens of nanoseconds later compared to other works [36].

The measurements of path-integrated magnetic fields were conducted during plasma expansion times from 10 to 40 ns. We have observed distinct field dynamics, both in the absolute value at the midpoint ($x = 0$) and in lateral extent, as shown in Fig. 3. The major axis, denoted as b, increased from 1 ± 0.2 mm at 10 ns to a maximum of 2.5 ± 0.3 mm at 30 ns and remained at 2.3 ± 0.3 mm at 40 ns. In contrast, the minor axis a fluctuated between 1.0 mm and 1.6 mm $\pm$ 0.1 mm, suggesting that the main effect of cavity growth occurred predominantly in one direction. The maximum cavity size is reached at 30 ns, typically referred to as the "time to peak diamagnetism," τ_d [23,26]. The velocity of the cavity expansion can be calculated by $v_d = (R_{b_{30}} - R_{b_{10}})/\Delta t = 7.5 \pm 0.6 \times 10^6$ cm/s, where $R_{b_{30}}$ and $R_{b_{10}}$ are the sizes of the cavity at 30 and 10 ns, Δt is the time difference, and R_b is b. This gives us a $\rho_i = 0.25$ mm for H ($Z_i = 1$) ions and $\rho_i = 0.5$ mm for C ions ($Z_i = 6$). Hence, we can determine a ratio of $\rho_i/R_b \approx 0.1 - 0.2$, which defines the magnetization of ions during the expansion [37].

To characterize the plasma conditions in the center of the diamagnetic cavity, we measured the electron temperatures and densities at 20 ns and 30 ns plasma expansion using 2ω OTS. We inferred a density of $n_e \approx 4 \pm 2 \times 10^{17}$ cm^{-3} and an electron temperature of $T_e \approx 45 \pm 15$ eV from the best fit to the electron plasma wave (EPW) spectrum.

By using the experimentally measured electron temperature and cavity size, we can calculate the time for the magnetic field to diffuse into the cavity, given by $\tau_{\text{diff}} = \mu_0 R_{b_{30}}^2/\eta$, where $R_{b_{30}}$ is the measured cavity size at the peak of diamagnetism, μ_0 is the vacuum permeability, and η is the electric resistivity for plasma at a given T_e. For a T_e of 45 ± 15 eV we find $\eta = 2 - 4 \times 10^{-6}$ Ωm [38] and $\tau_{\text{diff}} = 1.8 \pm 0.7$ μs. The diffusion time is much longer than the observed τ_{d} and consistent with previous diamagnetic cavity observations [26].

III. MAGNETO-HYDRODYNAMIC SIMULATIONS

The experimental data were compared with 3D single fluid magnetohydrodynamic simulations performed using the GORGON code [39,40]. Similar to previous works [14,15], the simulated domain (L_x, L_y, L_z) extended over ($10 \times 10 \times 20$) mm with a resolution of 20 μm and a numerical vacuum cutoff density set to 10^{-4} kg m^{-3}. The initial interaction of the

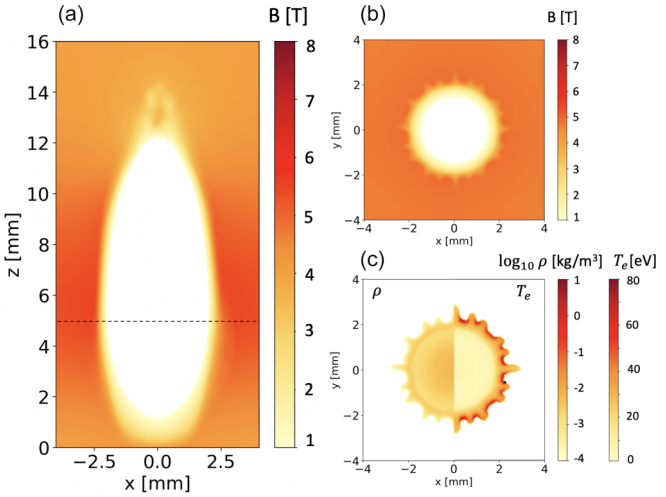

FIG. 4. GORGON MHD simulations of plasma expansion, shown at 20 ns expansion time. The *xyz* coordinates are the same as in the experiment. (a) Magnetic field in a cut through the middle of the computation domain in the *xz* plane. (b) Magnetic field and (c) density (left) and temperature (right) in a cut at $z = 5$ mm [black dashed line in (a)] in the *xy* plane, chosen to match the experimental distance from the plasma source to the midpoint of the height of the magnetic field coils.

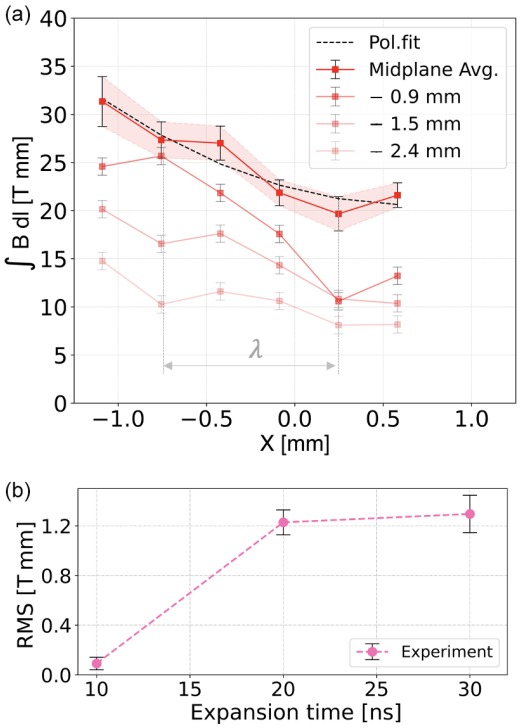

FIG. 5. (a) 1D $\int Bdl_{3\mathrm{MeV}}$ as a function of position x along the deflection axis extracted at midplane and at $Z = -0.9$, -1.5, and -2.4 mm along the plasma flow. The individual curves have been offset vertically for clarity. The $\int Bdl_{3\mathrm{MeV}}$ is averaged over three midplane beamlet rows. The error bar consists of the standard deviation of the signal for each point and a systematic error of 0.9 T. A polynomial fit with n = 2 was used to fit the expected curve shape. (b) δB_{rms} as a function of expansion time. The errors bars are estimated from $\int Bdl_{3\mathrm{MeV}}$ error bars by using Monte Carlo error analysis.

laser with the CH target was simulated using the radiation-hydrodynamic code DUED [41] in 2D axisymmetric geometry, and the resulting output was imported into GORGON. The initial magnetic field B_z was set to a uniform 5 T over the simulation box.

The simulation results are presented in Fig. 4. We observe a diamagnetic cavity maximum confinement radius of $R_{\text{b-sim}} = 3$ mm at $\tau_{d-\text{sim}} = 17$ ns expansion time, which compares to $R_{\text{b-exp}} = 2.5 \pm 0.3$ mm and $\tau_{d-\text{exp}} = 30$ ns. The spatial extent of the cavity is in good agreement with experiment, while the time to achieve the "peak of diamagnetism" is 10 ns faster. The cavity appears round, unlike the experimentally inferred elliptical shape, which can be explained by the nonuniform magnetic field generated by MIFEDS. The cavity expands with a velocity of $v_{d-\text{sim}} = 1.7 \times 10^7$ cm/s, twice as fast as observed in the experiment. The simulated electron density in the center of the cavity $n_{e-\text{sim}} \approx 2 \times 10^{17}$ cm^{-3} is reasonably consistent with OTS measurements, while the simulated $T_{e-\text{sim}} \approx 10$ eV is lower than the measured T_e. The higher measured T_e may be partially explained by OTS beam heating.

IV. GROWTH OF MAGNETO-RAYLEIGH TAYLOR INSTABILITIES

The flutelike structures observed at the edge of the simulated cavity are also evident in experimental observations conducted using proton radiography with 3 MeV protons. Figure 1(c) shows both raw and post-processed proton radiography images obtained with 3 MeV protons at a 20 ns expansion time. The 1D path integrated magnetic field $\int Bdl_{3\mathrm{MeV}}$ calculated from the beamlet deflections shown in Fig. 5(a) reveals fluctuations with a wavelength in the range of $\lambda_{\text{exp}} \approx 1.2 \pm 0.2$ mm. The oscillations in $\int Bdl_{3\mathrm{MeV}}$ are larger than error bars. The persistent wiggly features observed in $\int Bdl_{3\mathrm{MeV}}$ along the z axis suggest that these structures are elongated parallel to the plasma flow and the magnetic field. The structures are not observable with corresponding $\int Bdl_{15\mathrm{MeV}}$ protons in Fig. 3 (red curve) because 15 MeV protons are less sensitive to small magnetic field fluctuations compared to 3 MeV protons.

To evaluate the growth of these perturbations, we used a fit to the expected cavity shape at each expansion time. The signal perturbation to the cavity's shape can be evaluated by the root mean square of $\delta B_{\mathrm{rms}} = \sqrt{(B - B_{\mathrm{fit}})^2}$, where B is an experimental measurement and B_{fit} is a polynomial fit to the curve. The resulting δB_{rms} as a function of plasma expansion time is shown in Fig. 5(b). Using $\gamma_{\text{exp}} = 1/\Delta t \times \ln(\delta B_{\mathrm{rms}20}/\delta B_{\mathrm{rms}10}) = 0.25\,\mathrm{ns}^{-1}$ to define a growth rate, we find the growth time of the perturbations is $\tau_{\text{exp}} = 1/\gamma_{\text{exp}} = 3.8$ ns. The experimentally measured wavelength and growth time are in good agreement with the GORGON simulations, where we observe $\lambda_{\text{sim}} \approx 1$ mm and $\tau_{\text{sim}} = 1/\gamma_{\text{sim}} = 4.3$ ns.

To confirm the MRT nature of observed instability, we have compared our experimental and simulation results with analytic MRT theory. There are two analytic MRT approximations in the limits of $k \gg \epsilon_n$ and $k \ll \epsilon_n$. Here, $k = 2\pi/\lambda$ represents the wave number, and $\epsilon_n = d(\log n)/dx$ is the inverse density scale length. In our case, we have $k = 52\,\mathrm{cm}^{-1}$

and $\epsilon_n = 70\,\mathrm{cm}^{-1}$, as inferred from GORGON simulations. The expressions to estimate the MRT growth rate are as follows: $\gamma_{k\gg\epsilon_n} \approx \sqrt{(g_{\max}\epsilon_n)}$ [2,4], yielding a value of $1.87 \times 10^8\ \mathrm{s}^{-1}$ and $\gamma_{k\ll\epsilon_n} \approx \sqrt{gk}$ [22], yielding a value of $1.61 \times 10^8\ \mathrm{s}^{-1}$. The experimental deceleration rate of the cavity edge is estimated by $g_{\max} = 3/2V_d^2/R_b \approx 5 \times 10^{14}\,\mathrm{cm/s}^2$. The growth times are approximately $\tau_{k\gg\epsilon_n} \approx 5.3$ ns and $\tau_{k\ll\epsilon_n} \approx 6.2$ ns, respectively. These values are close to the simulated value of $\tau_{\mathrm{sim}} \approx 4.2$ ns and the experimental value of $\tau_{\mathrm{exp}} \approx 3.8$ ns.

We also have considered a MRT approximation, which includes viscosity and resistive diffusion, and depends on plasma temperature. Previous work has suggested that these effects may lead to the stabilization of MRT modes [14]. The MRT growth rate is given by $\gamma_{MRT} \sim \sqrt{gk} - k^2(\nu + D_M)$, where ν represents kinematic viscosity, and D_M is the magnetic diffusivity [42]. We measure a temperature of 45 eV at the center of the cavity. Simulations [Fig. 4(c)] indicate the temperature at the cavity edge to be several times higher than at the center. At such temperatures the viscosity and diffusivity term, $k^2(\nu + D_M)$, is negligible compared to $\sqrt{gk}$ (<10%) and little stabilization is predicted.

In summary, we have presented the first direct two-dimensional magnetic field measurements in the regime of $\rho_i/R_b \approx 0.1$. We have measured diamagnetic cavity dynamics and generation of unstable flutelike modes, identified as the MRT instability. The observed maximum spatial extent of the cavity agrees with 3D GORGON MHD simulations, though the time to reach peak diamagnetism occurs 10 ns later. The experimentally measured MRT wavelengths of 1.2 mm and growth rate of 3.8 ns are in good agreement with simulations. The overall comparison of results with the analytical MRT approximations suggests the importance of temperature and resistivity effects at the edge of the cavity.

ACKNOWLEDGMENTS

This work was supported through DOE Laboratory Directed Research and Development at Princeton Plasma Physics Laboratory, operated by Princeton University for the U.S. Department of Energy under Contract No. DE-AC02-09CH11466. The experiment was conducted at the Omega Laser Facility with the beam time through the Laboratory Basic Science under the auspices of the U.S. DOE/NNSA by the University of Rochester's Laboratory for Laser Energetics under Contract No. DE-NA0003856. This work was granted access to the HPC resources of MesoPSL financed by the Region Ile de France and the project EquipMeso (reference ANR-10-EQPX29-01) of the programme Investissements d'Avenir supervised by the Agence Nationale pour la Recherche. We would like also to thank J. Davies. A. Bhattacharjee, D. Winske, and P. Heuer for valuable discussions.

[1] A. Valenzuela, G. Haerendel, H. Föppl, F. Melzner, H. Neuss, E. Rieger, J. Stöcker, O. Bauer, H. Höfner, and J. Loidl, The "AMPTE" artificial comet experiments, Nature (London) **320**, 700 (1986).

[2] A. B. Hassam and J. D. Huba, Structuring of the "AMPTE" magnetotail barium releases, Geophys. Res. Lett. **14**, 60 (1987).

[3] A. B. Hassam and J. D. Huba, Magnetohydrodynamic equations for systems with large Larmor radius, Phys. Fluids **31**, 318 (1988).

[4] D. Winske, Development of flute modes on expanding plasma clouds, Physics of Fluids B: Plasma Physics **1**, 1900 (1989).

[5] P. M. Nilson, L. Willingale, M. C. Kaluza, C. Kamperidis, S. Minardi, M. S. Wei, P. Fernandes, M. Notley, S. Bandyopadhyay, M. Sherlock, R. J. Kingham, M. Tatarakis, Z. Najmudin, W. Rozmus, R. G. Evans, M. G. Haines, A. E. Dangor, and K. Krushelnick, Magnetic reconnection and plasma dynamics in two-beam laser-solid interactions, Phys. Rev. Lett. **97**, 255001 (2006).

[6] C. K. Li, F. H. Séguin, J. A. Frenje, J. R. Rygg, R. D. Petrasso, R. P. J. Town, O. L. Landen, J. P. Knauer, and V. A. Smalyuk, Observation of megagauss-field topology changes due to magnetic reconnection in laser-produced plasmas, Phys. Rev. Lett. **99**, 055001 (2007).

[7] G. Fiksel, W. Fox, A. Bhattacharjee, D. H. Barnak, P. Y. Chang, K. Germaschewski, S. X. Hu, and P. M. Nilson, Magnetic reconnection between colliding magnetized laser-produced plasma plumes, Phys. Rev. Lett. **113**, 105003 (2014).

[8] M. J. Rosenberg, C. K. Li, W. Fox, A. B. Zylstra, C. Stoeckl, F. H. Séguin, J. A. Frenje, and R. D. Petrasso, Slowing of magnetic reconnection concurrent with weakening plasma inflows and increasing collisionality in strongly driven laser-plasma experiments, Phys. Rev. Lett. **114**, 205004 (2015).

[9] C. Niemann, W. Gekelman, C. G. Constantin, E. T. Everson, D. B. Schaeffer, A. S. Bondarenko, S. E. Clark, D. Winske, S. Vincena, B. Van Compernolle, and P. Pribyl, Observation of collisionless shocks in a large current-free laboratory plasma, Geophys. Res. Lett. **41**, 7413 (2014).

[10] D. B. Schaeffer, E. T. Everson, A. S. Bondarenko, S. E. Clark, C. G. Constantin, D. Winske, W. Gekelman, and C. Niemann, Experimental study of subcritical laboratory magnetized collisionless shocks using a laser-driven magnetic piston, Phys. Plasmas **22**, 113101 (2015).

[11] D. B. Schaeffer, W. Fox, D. Haberberger, G. Fiksel, A. Bhattacharjee, D. H. Barnak, S. X. Hu, and K. Germaschewski, Generation and evolution of high-Mach-number laser-driven magnetized collisionless shocks in the laboratory, Phys. Rev. Lett. **119**, 025001 (2017).

[12] W. Yao, A. Fazzini, S. Chen, K. Burdonov, P. Antici, J. Béard, S. Bolaños, A. Ciardi, R. Diab, E. Filippov *et al.*, Laboratory evidence for proton energization by collisionless shock surfing, Nat. Phys. **17**, 1177 (2021).

[13] B. Albertazzi, A. Ciardi, M. Nakatsutsumi, T. Vinci, J. Béard, R. Bonito, J. Billette, M. Borghesi, Z. Burkley, S. N. Chen, T. E. Cowan, T. Herrmannsdörfer, D. P. Higginson, F. Kroll, S. A. Pikuz, K. Naughton, L. Romagnani, C. Riconda, G. Revet,

R. Riquier *et al.*, Laboratory formation of a scaled protostellar jet by coaligned poloidal magnetic field, Science **346**, 325 (2014).

[14] B. Khiar, G. Revet, A. Ciardi, K. Burdonov, E. Filippov, J. Béard, M. Cerchez, S. N. Chen, T. Gangolf, S. S. Makarov, M. Ouillé, M. Safronova, I. Y. Skobelev, A. Soloviev, M. Starodubtsev, O. Willi, S. Pikuz, and J. Fuchs, Laser-produced magnetic-Rayleigh-Taylor unstable plasma slabs in a 20 T magnetic field, Phys. Rev. Lett. **123**, 205001 (2019).

[15] A. Ciardi, T. Vinci, J. Fuchs, B. Albertazzi, C. Riconda, H. Pépin, and O. Portugall, Astrophysics of magnetically collimated jets generated from laser-produced plasmas, Phys. Rev. Lett. **110**, 025002 (2013).

[16] W. Yao, J. Capitaine, B. Khiar, T. Vinci, K. Burdonov, J. Béard, J. Fuchs, and A. Ciardi, Characterization of the stability and dynamics of a laser-produced plasma expanding across a strong magnetic field, Matter Radiat. Extremes **7**, 026903 (2022).

[17] D. Winske, J. D. Huba, C. Niemann, and A. Le, Recalling and updating research on diamagnetic cavities: Experiments, theory, simulations, Front. astron. space sci. **5**, 51 (2019).

[18] D. E. Ruiz, D. A. Yager-Elorriaga, K. J. Peterson, D. B. Sinars, M. R. Weis, D. G. Schroen, K. Tomlinson, J. R. Fein, and K. Beckwith, Harmonic generation and inverse cascade in the z-pinch driven, preseeded multimode, magneto-Rayleigh-Taylor instability, Phys. Rev. Lett. **128**, 255001 (2022).

[19] D. B. Sinars, S. A. Slutz, M. C. Herrmann, R. D. McBride, M. E. Cuneo, K. J. Peterson, R. A. Vesey, C. Nakhleh, B. E. Blue, K. Killebrew, D. Schroen, K. Tomlinson, A. D. Edens, M. R. Lopez, I. C. Smith, J. Shores, V. Bigman, G. R. Bennett, B. W. Atherton, M. Savage *et al.*, Measurements of magneto-Rayleigh-Taylor instability growth during the implosion of initially solid al tubes driven by the 20-ma, 100-ns Z facility, Phys. Rev. Lett. **105**, 185001 (2010).

[20] S. A. Slutz, M. C. Herrmann, R. A. Vesey, A. B. Sefkow, D. B. Sinars, D. C. Rovang, K. J. Peterson, and M. E. Cuneo, Pulsed-power-driven cylindrical liner implosions of laser preheated fuel magnetized with an axial field, Phys. Plasmas **17**, 056303 (2010).

[21] D. D. Ryutov, M. S. Derzon, and M. K. Matzen, The physics of fast z pinches, Rev. Mod. Phys. **72**, 167 (2000).

[22] E. G. Harris, Rayleigh-Taylor instabilities of a collapsing cylindrical shell in a magnetic field, Phys. Fluids **5**, 1057 (1962).

[23] B. H. Ripin, J. D. Huba, E. A. McLean, C. K. Manka, T. Peyser, H. R. Burris, and J. Grun, Sub-Alfvénic plasma expansion, Phys. Fluids B: Plasma Physics **5**, 3491 (1993).

[24] A. N. Mostovych, B. H. Ripin, and J. A. Stamper, Laser produced plasma jets: Collimation and instability in strong transverse magnetic fields, Phys. Rev. Lett. **62**, 2837 (1989).

[25] P. V. Heuer, M. S. Weidl, R. S. Dorst, D. B. Schaeffer, A. S. Bondarenko, S. K. P. Tripathi, B. Van Compernolle, S. Vincena, C. G. Constantin, C. Niemann, and D. Winske, Observations of a field-aligned ion/ion-beam instability in a magnetized laboratory plasma, Phys. Plasmas **25**, 032104 (2018).

[26] A. Collette and W. Gekelman, Structure of an exploding laser-produced plasma, Phys. Plasmas **18**, 055705 (2011).

[27] G. Dimonte and L. G. Wiley, Dynamics of exploding plasmas in a magnetic field, Phys. Rev. Lett. **67**, 1755 (1991).

[28] T. R. Boehly, R. S. Craxton, T. H. Hinterman, J. H. Kelly, T. J. Kessler, S. A. Kumpan, S. A. Letzring, R. L. McCrory, S. F. B. Morse, W. Seka, S. Skupsky, J. M. Soures, and C. P. Verdon, The upgrade to the OMEGA laser system, Rev. Sci. Instrum. **66**, 508 (1995).

[29] G. Fiksel, A. Agliata, D. Barnak, G. Brent, P. Y. Chang, L. Folnsbee, G. Gates, D. Hasset, D. Lonobile, J. Magoon, D. Mastrosimone, M. J. Shoup, and R. Betti, Note: Experimental platform for magnetized high-energy-density plasma studies at the OMEGA laser facility, Rev. Sci. Instrum. **86**, 016105 (2015).

[30] D. H. Froula, J. S. Ross, B. B. Pollock, P. Davis, A. N. James, L. Divol, M. J. Edwards, A. A. Offenberger, D. Price, R. P. J. Town, G. R. Tynan, and S. H. Glenzer, Quenching of the nonlocal electron heat transport by large external magnetic fields in a laser-produced plasma measured with imaging Thomson scattering, Phys. Rev. Lett. **98**, 135001 (2007).

[31] D. B. Schaeffer, A. F. A. Bott, M. Borghesi, K. A. Flippo, W. Fox, J. Fuchs, C. Li, F. H. S'eguin, H.-S. Park, P. Tzeferacos, and L. Willingale, Proton imaging of high-energy-density laboratory plasmas, Rev. Mod. Phys. **95**, 045007 (2023).

[32] F. H. Séguin, J. A. Frenje, C. K. Li, D. G. Hicks, S. Kurebayashi, J. R. Rygg, B.-E. Schwartz, R. D. Petrasso, S. Roberts, J. M. Soures, D. D. Meyerhofer, T. C. Sangster, J. P. Knauer, C. Sorce, V. Y. Glebov, C. Stoeckl, T. W. Phillips, R. J. Leeper, K. Fletcher, and S. Padalino, Spectrometry of charged particles from inertial-confinement-fusion plasmas, Rev. Sci. Instrum. **74**, 975 (2003).

[33] C. L. Johnson, S. Malko, W. Fox, D. B. Schaeffer, G. Fiksel, P. J. Adrian, G. D. Sutcliffe, and A. Birkel, Proton deflectometry with in situ x-ray reference for absolute measurement of electromagnetic fields in high-energy-density plasmas, Rev. Sci. Instrum. **93**, 023502 (2022).

[34] S. Malko, C. Johnson, D. B. Schaeffer, W. Fox, and G. Fiksel, Design of proton deflectometry with in situ x-ray fiducial for magnetized high-energy-density systems, Appl. Opt. **61**, C133 (2022).

[35] N. L. Kugland, D. D. Ryutov, C. Plechaty, J. S. Ross, and H. S. Park, Invited Article: Relation between electric and magnetic field structures and their proton-beam images, Rev. Sci. Instrum. **83**, 101301 (2012).

[36] C. A. Cecchetti, M. Borghesi, J. Fuchs, G. Schurtz, S. Kar, A. Macchi, L. Romagnani, P. A. Wilson, P. Antici, R. Jung, J. Osterholtz, C. A. Pipahl, O. Willi, A. Schiavi, M. Notley, and D. Neely, Magnetic field measurements in laser-produced plasmas via proton deflectometry, Phys. Plasmas **16**, 043102 (2009).

[37] Y. Zakharov, A. Orishich, A. G. Ponomarenko, and V. G. Posukh, Effectiveness of the slowing of expanding clouds of diamagnetic plasma by a magnetic field (experimental), Sov. J. Plasma Phys. **2**, 674 (1986) [Fiz. Plazmy **12**, 1170 (1986)].

[38] L. Spitzer, *Physics of Fully Ionized Gases* (Interscience Publishers, New York, 1956).

[39] J. P. Chittenden, S. V. Lebedev, C. A. Jennings, S. N. Bland, and A. Ciardi, X-ray generation mechanisms in three-dimensional simulations of wire array z-pinches, Plasma Phys. Controlled Fusion **46**, B457 (2004).

[40] A. Ciardi, S. V. Lebedev, A. Frank, E. G. Blackman, J. P. Chittenden, C. J. Jennings, D. J. Ampleford, S. N. Bland, S. C.

Bott, J. Rapley, G. N. Hall, F. A. Suzuki-Vidal, A. Marocchino, T. Lery, and C. Stehle, The evolution of magnetic tower jets in the laboratorya), Phys. Plasmas **14**, 056501 (2007).

[41] S. Atzeni, A. Schiavi, F. Califano, F. Cattani, F. Cornolti, D. Del Sarto, T. Liseykina, A. Macchi, and F. Pegoraro, Fluid and kinetic simulation of inertial confinement fusion plasmas, Comput. Phys. Commun. **169**, 153 (2005), Proceedings of the Europhysics Conference on Computational Physics 2004.

[42] T. Green and G. Niblett, Rayleigh-Taylor instabilities of a magnetically accelerated plasma, Nucl. Fusion **1**, 42 (1960).